2017 IEEE/RSJ International Conference on Intelligent Robots and Systems (IROS)
September 24–28, 2017, Vancouver, BC, Canada

Generalized Hebbian Algorithm for Wearable Sensor Rotation Estimation

Vladimir Joukov, Jonathan Feng-Shun Lin, and Dana Kulić

Abstract— **Inertial measurement units (IMUs) enable human motion measurement in any environment, which can be useful for human robot interaction, exoskeletons, and active prosthetics. This paper proposes an approach for estimating the orientation between a wearable IMU sensor and the body frame of the wearer using a simple and fast calibration procedure. The proposed approach uses the generalized Hebbian algorithm to incrementally estimate the axis aligned with gravity using acceleration measurements obtained during a static pose, and the axis perpendicular to the saggital plane using gyro measurements obtained during sagittal plane movements. An automated convergence criterion based on the sensor measurement variance is used. The proposed approach is tested in simulation and with human movement and demonstrates excellent and fast calibration performance.**

I. Introduction

In many applications including human-robot interaction, to minimize risk of injury and provide the best assistance in collaborative tasks, the robot must have an excellent estimate of the human's pose [1]. Camera based motion capture systems are the gold standard for human motion measurement, however these systems are expensive, can only be used in indoor environments, and suffer from occlusions. On the other hand, wearable inertial measurement units (IMUs) can be used in cluttered indoor or outdoor environments. However, while camera systems measure body worn markers with respect to a global frame, each wearable IMU provides measurements in its local frame. To achieve accurate human pose estimation using wearable IMUs, it is imperative to have excellent alignment between the IMU and body frames [2].

Pose estimation techniques that are sensitive to alignment errors include methods employing accelerometers as 1D inclinometers during slow motion [3], [4] and switching to gyroscope integration during fast motion [5], [6]. The Kalman filter, a common sensor fusion technique that estimates body joint angles via the kinematic model and sensor noise covariance, is also sensitive to sensor alignment errors [7], [8], [9] as the kinematic model requires the sensor orientation to be known. Despite its importance, sensor frame alignment for human motion estimation is generally assumed to be achieved via careful sensor placement by all of the above cited methods.

In addition to human motion applications, the alignment between the IMU and body frames has been considered for automotive applications, where the offset between the IMU frame and the vehicle frame is of interest [10], [11], [12].

Prior methods for sensor frame alignment fall into four major categories, and rely on either known motions or motion capture to provide the information needed for calibration.

The first set of techniques utilizes the Kalman filter, a sensor fusion method that combines a state model with a measurement model to produce a state estimate. Yang and Ye [13] use a series of known motions in a Kalman filter framework, with the state being the orientation of gravity, the measurement being acceleration, and the control signal the gyroscope. From a pre-defined stationary pose, the Kalman filter is used to calculate the direction of gravity, which determines one of the axes. With a set of planar movements, the second axis can be set to be aligned with the direction of movement. The last axis is set to be orthogonal to the second via the cross-product.

The second set of techniques utilize principal component analysis (PCA) to determine the axes of movement. PCA is a statistical method that rotates the features of a dataset into a space such that the new features are ordered by the amount of variance present in the dataset as a linear combination of the original feature space. Basir *et al.* [14] proposed a technique for IMU to vehicle frame alignment using measurement of the gravity vector by the accelerometer to determine the vertical axis when the vehicle is at rest. Using PCA, the linear acceleration of forward movement can be used to determine a second axis, while the last axis is orthogonal to the two. Kong *et al.* [15] utilize a similar technique, using predetermined sagittal plane motions with PCA to obtain the second axis. Variants of this technique, where PCA is applied to the angular velocity of the vehicle turning movements to determine the second axis, have also been proposed [16], [12].

The third set of techniques relies on optimization methods to estimate the alignment matrix with respect motion capture data. Chardonnens *et al.* [17] applied nonlinear optimization to obtain the alignment matrix, by minimizing the error between the joint angles obtained from integrating the gyroscope signal and those obtained from the motion capture system. de Vries *et al.* [18] propose a least squares approach to determine the alignment matrix to minimize the error between the angular velocity of motion capture markers on the IMU and the IMU gyroscope data.

The last set of techniques use the Kronecker product and singular value decomposition (SVD) to obtain alignment with respect to motion capture data. Shah [19] showed that SVD of the Kronecker product of the matrices describing the rotations from the start of the motion to the current frame in the IMU and motion capture frames can be used to calculate the alignment matrix.

In this paper we propose a novel approach to estimate the rotation matrix between the IMU and body frames, using an iterative algorithm based on the Generalized Hebbian

978-1-5386-2681-8/17/$31.00 ©2017 IEEE

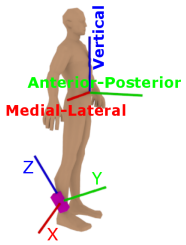

Fig. 1. The human body and IMU frames for a shank worn IMU.

Algorithm (GHA) [20]. The method runs on-line and to be used with small wearable sensors that may not have large data storage capabilities. Furthermore, the algorithm automatically detects when an accurate rotation matrix has been estimated, minimizing calibration time, which is critical in real world applications. We compare the proposed approach to the PCA accelerometer based method described in [15]. The results show that on real human data the proposed method significantly improves the rotation matrix estimate.

II. Proposed Approach

For accurate kinematic based pose estimation from wearable IMUs, it is important to obtain the relationship between the frame of the sensor measurements and the kinematic model frame without relying on motion capture. Thus we have to find the rotation matrix ${}^{link}_{s}R$ from the sensor frame to the frame of the kinematic link it is attached to. Equivalently we need to determine the orientation of each axis of the link frame in the sensor frame. We focus on estimating the orientation of a shank worn IMU, but the same approach is easily extended to any link. Defining the body frame with index 0, with the $[x_0,\ y_0,\ z_0]$ axes corresponding to the medial-lateral, anterior-posterior, and vertical directions respectively, our goal is to find the representation of each of the axes in the IMU frame:

$$ {}^{0}_{s}R = {}^{s}_{0}R^{T} = [{}^{s}x_0,\ {}^{s}y_0,\ {}^{s}z_0]^{T}. \tag{1} $$

The proposed method works in two stages: First the ${}^{s}z_0$ component is estimated during a static pose. Second, a planar motion is used to estimate the ${}^{s}x_0$ and ${}^{s}y_0$ components. A practical calibration procedure has to be fast and it should terminate automatically when the rotation matrix estimate is accurate. We propose to use the GHA [20] to iteratively learn an accurate estimate of the components in both stages. The approach automatically terminates the calibration procedure when the rotation matrix estimate is accurate.

A. Generalized Hebbian Algorithm

The GHA [20] can be used to iteratively estimate the principal components of incoming data. It updates each eigenvector estimate by adding to it the input vector minus the projection of the input vector onto each of the other eigenvectors. At each iteration, given a data sample v, the i_{th} principal component c_i is updated as follows:

$$ \Delta c_i = c_i \cdot v(v - \sum_{j<i}(v \cdot c_j)c_j) \tag{2} $$

$$ c_i = c_i + \eta \Delta c_i \tag{3} $$

where η is the learning rate. The algorithm converges to the exact eigenvector decomposition of the data with a probability of one. Assuming that the eigenvectors are not changing, c_i and Δc_i will be in the same direction when convergence is achieved. Thus their normalized difference can be used as a measure of convergence.

$$ m_c = \| \frac{c_i}{\|c_i\|} - \frac{\Delta c_i}{\|\Delta c_i\|} \| \tag{4} $$

B. Estimating ${}^{s}z_0$

Considering the accelerometer measurement $a_{imu} = [a_x\ a_y\ a_z]$ during a static pose, only gravity is measured and the accelerometer's first principal component will be in the ${}^{s}z_0$ direction. Thus it is possible to use the GHA to converge to an accurate estimate of the ${}^{s}z_0$. Normalizing the component at each iteration ensures the estimate remains a unit vector, a necessary condition for estimating a proper rotation matrix ${}^{0}_{s}R$. To detect when the component is accurately estimated, we propose to use the standard deviation of the normalized stationary accelerometer signal. At each iteration of GHA we expect $\frac{1}{3}$ of the accelerometer sensor noise to be along the Δc_i and $\frac{2}{3}$ in the two perpendicular axes. Thus it is possible to use the standard deviation of the accelerometer signal as a threshold on the convergence measure (equation 4). The algorithm is outlined below as algorithm 1, where the learning rate η_a and desired number of points K are two tuning parameters for the ${}^{s}z_0$ component estimation. The learning rate is set such that the convergence is desirably fast but the component estimate is not greatly affected by sensor noise at each iteration. Waiting for a desired number of points below the accelerometer convergence metric m_a threshold ensures that the component converges.

Algorithm 1 GHA ${}^{s}z_0$ Estimation

Initialize:
  ${}^{s}z_0 \leftarrow [0\ 0\ 1]^T$
  $K = 0$
while K<*Desired Number of Points* **do**
  $x = \frac{a_{imu}}{\|a_{imu}\|}$
  $\Delta\,{}^{s}z_0 = {}^{s}z_0 \cdot x(x)$
  ${}^{s}z_0 = {}^{s}z_0 + \eta_a \Delta\,{}^{s}z_0$
  ${}^{s}z_0 = \frac{{}^{s}z_0}{\|{}^{s}z_0\|}$
  $m_a = \|{}^{s}z_0 - \frac{\Delta\,{}^{s}z_0}{\|\Delta\,{}^{s}z_0\|}\|$
  if $m_a < \frac{2}{3} std(a_{imu})$ **then**
    $K = K + 1$
  end if
end while

C. Estimating ${}^s x_0$ and ${}^s y_0$

We now need to determine the ${}^s x_0$ and ${}^s y_0$ components of the rotation matrix. A planar motion such as flexion extension in the knee or hip will produce a rotation about the x_0 axis. Thus, the first principal component of the gyroscope measurements will be along the ${}^s x_0$ axis. Utilizing the fact that the z_s^s component is already known from the static pose estimate described in section II-B and that for a valid rotation matrix the ${}^s y_0$ axis must be perpendicular to both ${}^s z_0$ and ${}^s x_0$, we calculate ${}^s y_0$ using the cross product, ${}^s y_0 = {}^s z_0 \times {}^s x_0$. We apply the GHA while the participant is performing a planar motion. In this case we use the standard deviation of the gyroscope during the static pose to determine when convergence is achieved. The algorithm for estimating the two components using the gyroscope measurement $w_{imu} = [w_x,\ w_y,\ w_z]$ is shown in algorithm 2. The subtraction of gyroscope measurement projected onto the ${}^s z_0$ component ensures that ${}^s z_0$ and ${}^s x_0$ remain perpendicular. Note that gyroscope measurement is used without normalization, ensuring that $\Delta\, {}^s x_0$ is proportional to the angular velocity. Thus the ${}^s x_0$ component does not significantly change during low angular velocities when sensor noise is a dominant part of the signal. Human motion is unlikely to be exactly planar, however in some cases, such as walking in a straight line, the out of plane motion has zero mean. In this case the error in component estimation can be averaged out by applying SVD to the sum of estimated rotation matrices [21] after convergence over multiple motion cycles.

Algorithm 2 GHA ${}^s x_0$ and ${}^s y_0$ Estimation

Initialize:
  ${}^s x_0 \leftarrow [1\ 0\ 0]^T$
  ${}^s y_0 = {}^s z_0 \times {}^s x_0$
  $K = 0$
while $K < Desired\ Number\ of\ Points$ **do**
  $x = w_{imu} - w_{imu} \cdot {}^s z_0 ({}^s z_0)$
  $\Delta\, {}^s x_0 = {}^s x_0 \cdot x(x)$
  ${}^s x_0 = {}^s x_0 + \eta_w \Delta\, {}^s x_0$
  ${}^s x_0 = \frac{{}^s x_0}{\|{}^s x_0\|}$
  ${}^s y_0 = {}^s z_0 \times {}^s x_0$
  $m_g = \|{}^s x_0 - \frac{\Delta\, {}^s x_0}{\|\Delta\, {}^s x_0\|}\|$
  if $m_g < \frac{2}{3} std(w_{imu})$ **then**
    $K = K + 1$
  end if
end while
${}^0_s R \leftarrow [{}^s x_0,\ {}^s y_0,\ {}^s z_0]^T$

III. Validation Results

The proposed approach is evaluated in simulation, simulating a human performing a knee flexion extension exercise, and with real data of a seated knee flexion-extension exercise and human gait. In simulation we analyze the convergence of the GHA under different sensor orientation conditions. With the real data we compare directly the actual and estimated sensor rotation matrices. In order to establish the accuracy of the estimated rotation matrix, we use the inner product of unit quaternions. This metric represents the angle between two quaternions:

$$D(R_{act}, R_{est}) = 2cos^{-1}(q_{est} \cdot q_{act}) \tag{5}$$

Where q_{est} and q_{act} are the quaternion representations of the estimated and actual rotation matrices respectively.

For the real human motion data, we also compare the accuracy of the proposed approach to the accelerometer PCA method proposed in [15]. Their approach consists of a similar two step estimation process. However, it is not iterative and does not automatically terminate. First they estimate the ${}^s z_0$ component using the mean of the accelerometer signal during a static pose. Next, they apply PCA to both the accelerometer signal and a rotated set symmetric about the origin $[a_{imu}; -a_{imu}]$ for the entire planar motion dataset. The first two principal components represent the plane of motion and thus the cross product of ${}^s z_0$ and the plane's normal vector is the ${}^s y_0$ or $-\,{}^s y_0$ component. Finally, the ${}^s x_0$ component is computed as the cross product of ${}^s y_0$ and ${}^s z_0$. Note that this approach does not discriminate between ${}^s y_0$ or $-\,{}^s y_0$ while the proposed method will always converge to the solution closest to the initial guess of ${}^s x_0$. Furthermore, gyroscopes typically handle impacts better and are less noisy than accelerometers thus by relying on the gyroscope for ${}^s x_0$ and ${}^s y_0$ estimates we expect improved performance.

A. Simulation Validation

To test the convergence properties and estimation accuracy of the proposed approach we simulate a gyroscope and an accelerometer attached at an offset of 0.5 m to a spherical joint represented by 3 Euler angles. The sensors are rotated by 45 deg in roll, pitch, and yaw with respect to the joint frame. To simulate human gait, the joint is actuated with a sinusoidal motion of magnitude 45 deg about the x_0 axis coinciding with the first Euler angle at a frequency of 1 Hz. Out of plane motion with 5 deg magnitude is added to the other two Euler angles at a frequency of 2 Hz. Using forward kinematics, the sensor measurements are computed at a sampling rate of 100 Hz for 30 seconds of static pose and 30 seconds of motion, random Gaussian noise of $0.1\frac{m}{s^2}$ and $0.01\frac{rad}{s}$ is added to the accelerometer and gyroscope respectively. The learning rates η_a, η_w, and number of desired points K below threshold were chosen experimentally as 0.05, 0.001, and 20, respectively.

Figure 2 shows the convergence of the ${}^s z_0$ component using the algorithm described in section II-B. Figure 3 shows the convergence of the ${}^s x_0$ and ${}^s y_0$ components with and without out of plane motion, using the algorithm described in section II-C, after an estimate of ${}^s z_0$ is obtained. Table I compares the convergence time and accuracy with and without out of plane motion of the proposed approach with accelerometer PCA based method [15]. When no out of plane motion is present, given the learning rates and desired number of points under the threshold, the proposed approach converges in only 2.45 seconds. Using the entire 50 seconds the PCA method is able to provide better results. However,

TABLE I

COMPARISON OF PROPOSED APPROACH (GHA) WITH PCA[15].

	Planar		Non-Planar	
	GHA	PCA	GHA	PCA
Convergence Time (s)	**2.45**	60	**14.4**	60
Accuracy $D(R_{act}, R_{est})$	0.11	**0.03**	**2.62**	8.82

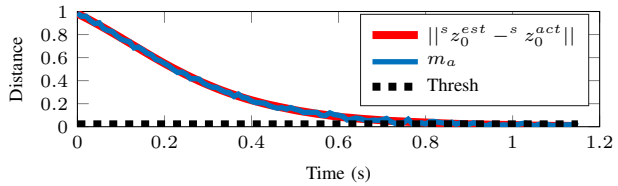

Fig. 2. Convergence of the ${}^s z_0$ component when the sensor is rotated 45 deg in roll, pitch, and yaw with respect to the link frame. Note that while the convergence metric m_a (blue) is susceptible to sensor noise the distance between actual and estimated ${}^s z_0$ components converges smoothly to zero. After only 1.2 seconds 20 samples fall below the convergence metric standard deviation threshold (black), the algorithm terminates with a final error of 2.5×10^{-3}.

when 5 degree out of plane motion is introduced the proposed approach is able to both quickly converge and significantly improve the estimation accuracy.

Next we look at the time it takes the proposed approach to converge to an accurate estimate over increasing sensor misalignment. We run multiple simulations without out of plane motion, in each simulation increasing the roll, pitch, and yaw in the sensor rotation matrix from 0 to 70 deg. Figure 4 shows the convergence times of the two algorithm steps plotted against the rotation matrix distance metric with respect to identity.

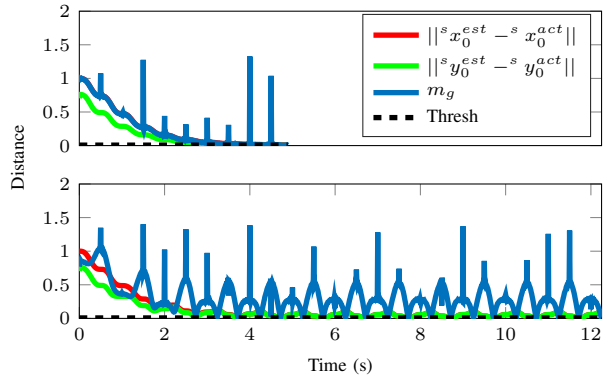

Fig. 3. Estimation of the ${}^s x_0$ and ${}^s y_0$ components without (top) and with (bottom) out of plane motion. The sensor is rotated 45 deg in roll, pitch, and yaw with respect to the link frame. The large peaks in the convergence metric occur when the joint is near zero velocity and sensor noise is the dominant sensor signal. However, because the update of the component at each iteration is proportional to the gyroscope measurement the component estimate is not affected in the near zero velocity regions. With significant out of plane motion (bottom) the component estimation oscillates about the true IMU axes. The proposed convergence metric is minimized when the estimated estimated IMU axes and instantaneous axes of rotation are aligned. The algorithm terminates after 12 seconds, the last iteration and svd of rotation matrix sum (${}^s x_0$ and ${}^s y_0$) components are estimated with (0.074, 0.074) and (0.042, 0.043) error norms respectively.

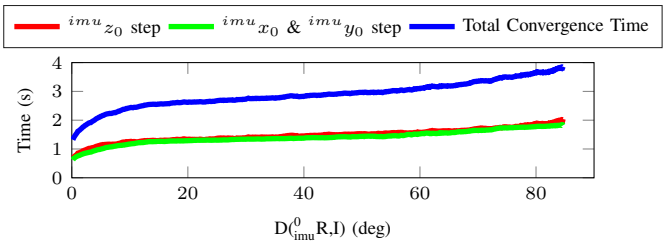

Fig. 4. Convergence times of the ${}^s z_0$ estimation (red), ${}^s x_0$ and ${}^s y_0$ (green) steps and total time (blue) at different sensor orientations. After a rotation offset of larger than 10 deg a linear increase in convergence time is observed.

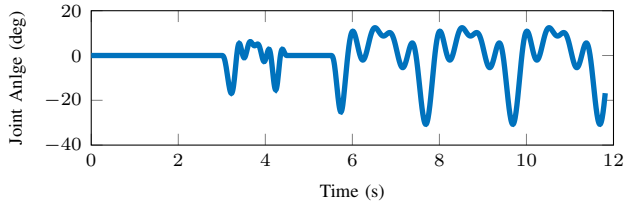

Fig. 5. Simulation of complex human motion. First, three seconds are used as the static interval. Next, a single motion repetition is generated as a sum of five sinusoids with random coefficients. The movement is paused from 4.5 to 5.5 seconds. Finally, three more movement repetitions are completed at double magnitude and half the frequency of the first.

In a practical scenario the human participant may not achieve perfectly sinusoidal motion, for example a rehabilitation patient may pause and restart their motion due to fatigue and perform movements of different magnitudes due to pain. To investigate the applicability of the proposed approach in such a scenario we generate a planar motion as a sum of five sinusoids with random magnitudes. After the first repetition the movement is paused for one second and later repeated at double the magnitude and half the frequency. Figure 5 shows the generated joint angle versus time.

As in the previous simulation experiment the IMU is rotated 45 deg in roll, pitch, and yaw with respect to the link frame and the measurements are generated using forward kinematics. The first three seconds are used to estimate ${}^s z_0$ component and the rest of the motion to estimate ${}^s x_0$ and ${}^s y_0$ components. Figure 6 shows the convergence of the ${}^s x_0$ and ${}^s y_0$ components during the complex motion.

B. Human Motion Validation

We next validate the proposed approach on real human data, estimating the rotation matrix between a single IMU placed on the inner shank and the body frame using a seated knee flexion-extension exercise and human gait. Orientation computed from motion capture markers is used as ground truth. The motion capture studio utilizes 8 Motion Analysis cameras capturing at 200 Hz. Our inertial measurement unit consists of the MPU9250 sensor and was set to sample at 100 Hz. The sensor was calibrated with the algorithm proposed in [22] prior to data collection. The proposed standard deviation convergence metric thresholds for m_a and m_g were determined as 0.010 and 0.017 respectively using 30 seconds

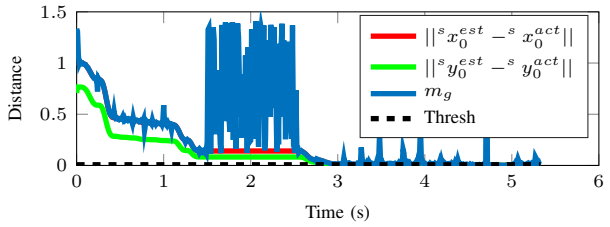

Fig. 6. Convergence of the ${}^s x_0$ and ${}^s y_0$ components during complex motion. The algorithm successfully converges on an accurate estimate of the components and does not update them during a pause in the movement, when gyroscope noise dominates the signal. After 6.5 seconds the ${}^s x_0$ and ${}^s y_0$ components are estimated with 2.1×10^{-3} and 8.2×10^{-4} error norms respectively.

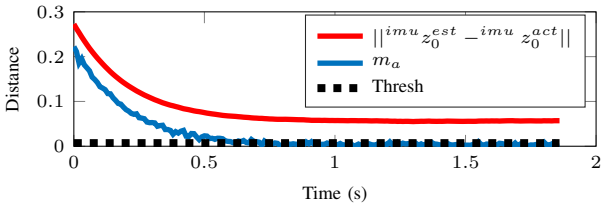

Fig. 7. Convergence of the ${}^s z_0$ component during static pose with real IMU data. Note there is a constant offset between the actual ${}^s z_0^{act}$ component computed using motion capture markers and the estimated ${}^s z_0^{est}$. The proposed approach converges to the gravity vector in the sensor frame, unfortunately, perfect alignment between the axes defined by markers placed on the IMU and real accelerometer axis is difficult. This misalignment is the cause of the constant offset between the motion capture based and estimated ${}^s z_0$ components.

of sensor data before it was attached to the participant. The same learning rates η_a, η_w and desired number of samples below threshold K were used as in section III-A.

1) Ground Truth Estimation: It was assumed that during static sitting and standing poses the body's vertical axis is aligned with the world z_w axis, thus ${}^w z_0 = [0,\ 0,\ 1]$. To identify the medial-lateral axis we placed a motion capture marker on the lateral side of the ankle bone. The medial-lateral axis has to be perpendicular to the vertical axis and any vector v_{ap} along the anterior posterior plane. We use the ankle marker position during full knee flexion to full knee extension and beginning to end of a gait cycle as such a vector for the flexion-extension and walking validations respectively. Then the medial-lateral axis is computed as the cross product of ${}^w z_0$ and v_{ap}, ${}^w x_0 = {}^w z_0 \times v_{ap}$. Finally the true anterior-posterior axis can be computed as the cross product of the medial-lateral and vertical axes, ${}^w y_0 = {}^w z_0 \times {}^w x_0$. This process provides us with the rotation matrix from world frame to the body frame ${}^0_w R = [{}^w x_0,\ {}^w y_0,\ {}^w z_0]$. Three motion capture markers are placed on the IMU and the method proposed in [17] is used to align the axes defined by the markers with the internal sensor measurement frame, allowing to compute ${}^w_s R$, leading us to a ground truth rotation matrix between the IMU and body frames:

$$R_{act} = {}^0_s R = {}^0_w R\ {}^w_s R \tag{6}$$

2) Flexion Extension Validation: A participant sat in a static pose for 30 seconds and then performed a seated knee flexion-extension exercise for one minute while wearing a single IMU mounted on the shank and motion capture markers at the hip, knee, and ankle. Figures 7 and 8 show the convergence of the rotation matrix.

The error metric comparison of the proposed approach and the accelerometer based PCA method in [15] which utilizes the entire 30 seconds of static data to estimate the ${}^s z_0$ and 60 seconds of motion to estimate the ${}^s x_0$ and ${}^s y_0$ components is provided in Table II.

3) Gait Validation: Standing upright and walking are easy and natural examples of static pose and planar motion. Thus, if the proposed approach can achieve accurate IMU to body orientation estimation from just standing and walking it can be utilized in multiple practical applications. We captured a

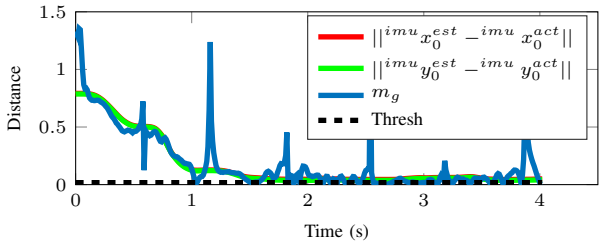

Fig. 8. Estimation of the ${}^s x_0$ and ${}^s y_0$ components during knee flexion-extension. Unlike the accelerometer, the gyroscope has significantly better alignment to the axes defined by the makers placed on the IMU and the ${}^s x_0$ and ${}^s y_0$ are accurately estimated with 0.048 and 0.041 error norms respectively.

participant standing upright for 30 seconds and then walking down a straight hallway for 60 seconds with their natural gait. The proposed approach converged to an accurate estimate of ${}^s z_0$ in just 1.6 seconds and on accurate estimate of ${}^s x_0$ and ${}^s y_0$ in only 12 seconds of gait. This is equivalent to 9 gait cycles as seen in figure 9. The proposed approach and the accelerometer based PCA method rotation matrix estimation accuracies are provided in table II.

C. Discussion

Since the estimation of ${}^s z_0$ of both methods relies on the static accelerometer measurement the results are similar in accuracy. The significant improvement in estimation is due

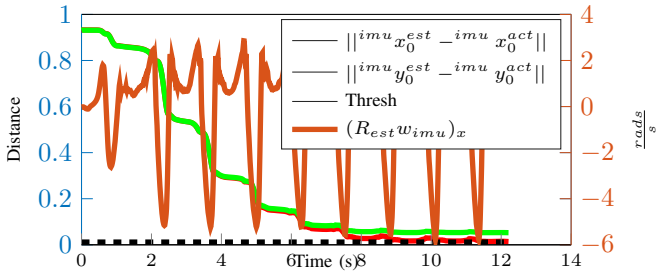

Fig. 9. Convergence of the ${}^s x_0$ and ${}^s y_0$ components during natural gait. After applying the estimated rotation to the gyroscope measurement we plot the angular velocity of the medial-lateral axis, the components converge in only 9 gait cycles.

TABLE II

ERROR METRIC AND INDIVIDUAL COMPONENT ERROR COMPARISON.

	Flex-Ext		Gait	
	GHA	PCA	GHA	PCA
$D(R_{act}, R_{est})$ (deg)	**3.4**	4.7	**3.1**	5.2
$\|{}^s x_0^{est} - {}^s x_0^{act}\|$	**0.049**	0.083	**0.014**	0.065
$\|{}^s y_0^{est} - {}^s y_0^{act}\|$	**0.042**	0.079	**0.053**	0.088
$\|{}^s z_0^{est} - {}^s z_0^{act}\|$	**0.057**	0.054	**0.054**	0.061

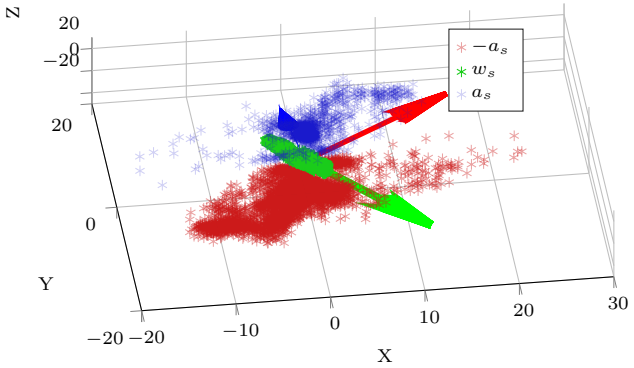

Fig. 10. 3D scatter plot of the accelerometer (blue), its rotated set symmetric about origin (red) and gyroscope (green) data during gait. Note only every fifth a_{imu} point is plotted to better see the gyroscope signal. The red and green arrowheads show the actual components of the rotation matrix. It is clear that the gyroscope principal direction is well aligned with ${}^s x_0$.

to the use of the gyroscope instead of the accelerometer to estimate the medial-lateral axis. For good estimation the PCA method requires the accelerometer data to lie on a plane, however, accelerometers are noisy and extremely susceptible to impacts. The 3d point cloud of the accelerometer and gyroscope signals (figure 10) shows that the gyroscope has significantly lower variability and thus is more suitable for estimation of the rotation matrix.

Although the proposed method outperforms [15], a key advantage of [15] is that it requires only accelerometer data, while the proposed approach requires both accelerometer and gyroscope data. While the availabity of gyroscope data is generally not an issue with modern IMUs, the proposed method also assumes that the intrinsic sensor calibration [22] provides good alignment between the accelerometer and the gyroscope frame. [15] avoids these issues by requiring only the accelerometer. The proposed method also used a motion capture-based technique [17] to generate the ground truth R_{act}. However, it is important to note that [17] reported an error of up to 1 deg, which may offset the error values reported for the proposed method.

IV. CONCLUSION

In this paper we proposed a novel iterative method to estimate the rotation matrix between a wearable inertial measurement unit and the body frame. Our two step approach utilizes the Generalized Hebbian Algorithm to first estimate the body vertical axis using accelerometer measurements during static pose and then the medial-lateral and anterior-posterior axes based on gyroscope measurements during planar motion. We introduced a measure of convergence based on the noise properties of the sensors allowing the algorithm to terminate automatically when it converges onto an accurate rotation matrix estimate. The algorithm has been validated in simulation and on real human data.

The results show that rotation alignment comparable to performance when motion capture is available can be achieved with this simple protocol, within a few seconds of easy to perform movement such as knee flexion extension or gait, making the approach suitable for calibration in field and clinical settings. For future work, the algorithm will be tested with a larger population of users, on different body segments, and with different exercises, to assess algorithm generalizability.

REFERENCES

[1] D. Kulić *et al.*, "Anthropomorphic movement analysis and synthesis: A survey of methods and applications," *IEEE Trans Robot*, vol. 32, pp. 776–95, 2016.

[2] M. Miezal *et al.*, "On inertial body tracking in the presence of model calibration errors," *Sensors*, vol. 16, 2016.

[3] J. Bergmann *et al.*, "A portable system for collecting anatomical joint angles during stair ascent: A comparison with an optical tracking device," *Dyn Med*, vol. 8, pp. 1–7, 2009.

[4] K. Low *et al.*, "A wearable wireless sensor network for human limbs monitoring," in *Instrumen Meas Tech Conf*, 2009, pp. 1332–6.

[5] M. Boonstra *et al.*, "The accuracy of measuring the kinematics of rising from a chair with accelerometers and gyroscopes," *J Biomech*, vol. 39, pp. 354–8, 2006.

[6] M. Ayoade *et al.*, "Investigating the feasibility of a wireless motion capture system to aid in the rehabilitation of total knee replacement patients," in *Conf Perv Compu Tech Health*, 2011, pp. 404–7.

[7] H. Luinge and P. Veltink, "Measuring orientation of human body segments using miniature gyroscopes and accelerometers," *Med Biol Eng Comput*, vol. 43, pp. 273–82, 2005.

[8] J. Lin and D. Kulić, "Human pose recovery using wireless inertial measurement units," *Physiol Meas*, vol. 33, pp. 2099–115, 2012.

[9] V. Joukov *et al.*, "Rhythmic ekf for pose estimation during gait," in *IEEE Conf Human Robots*, 2015, pp. 1167–72.

[10] J. Paefgen *et al.*, "Driving behavior analysis with smartphones: Insights from a controlled field study," in *Conf Mob Ubi Media*, 2012, pp. 36:1–8.

[11] G. Castignani *et al.*, "Driver behavior profiling using smartphones: A low-cost platform for driver monitoring," *IEEE Intell Transp Syst Mag*, vol. 7, pp. 91–102, 2015.

[12] C. Woo and D. Kulić, "Manoeuvre segmentation using smartphone sensors," in *IEEE Intell Veh Symp*, 2016, pp. 572–7.

[13] H. Yang and J. Ye, "A calibration process for tracking upper limb motion with inertial sensors," in *IEEE Conf Mech Autom*, 2011, pp. 618–23.

[14] O. Basir *et al.*, "Method of correcting the orientation of a freely installed accelerometer in a vehicle," 2013, US Patent App. 13/632,554.

[15] W. Kong *et al.*, "Anatomical calibration through post-processing of standard motion tests data," *Sensors*, vol. 16, 2016.

[16] R. Larsdotter and D. Jaller, "Automatic calibration and virtual alignment of mems-sensor placed in vehicle for use in road condition determination system," Master's thesis, Chalmers Univ Tech, 2014.

[17] J. Chardonnens *et al.*, "An effortless procedure to align the local frame of an inertial measurement unit to the local frame of another motion capture system," *J Biomech*, vol. 45, pp. 2297–300, 2012.

[18] W. de Vries *et al.*, "Magnetic distortion in motion labs, implications for validating inertial magnetic sensors," *Gait Posture*, vol. 29, pp. 535–41, 2009.

[19] M. Shah, "Solving the robot-world / hand-eye calibration problem using the kronecker product," *J Mech Robot*, vol. 5, p. 031007, 2013.

[20] T. Sanger, "Optimal unsupervised learning in a single-layer linear feedforward neural network," *Neural networks*, vol. 2, pp. 459–73, 1989.

[21] I. Sharf *et al.*, "Arithmetic and geometric solutions for average rigid-body rotation," *Mechanism and Machine Theory*, vol. 45, no. 9, pp. 1239–251, 2010.

[22] D. Tedaldi *et al.*, "A robust and easy to implement method for imu calibration without external equipments," in *IEEE Conf Robot Autom*, 2014, pp. 3042–9.